



Research Article

A search for 3-mm molecular absorption line transitions in the magellanic stream

Lucille Steffes¹ , Daniel R. Rybarczyk¹, Snežana Stanimirović¹, J. R. Dawson^{2,3} , Mary Putman⁴, Philipp Richter⁵, John Gallagher III¹, Harvey Liszt⁶, Claire Murray^{1,7}, John Miller Dickey⁸, Carl Heiles⁹, Audra Hernandez¹, Robert Lindner¹, Yangyang Liu^{1,10}, Naomi M. McClure-Griffiths¹¹, Tony Wong¹² and Blair Savage^{1,13}

¹Department of Astronomy, University of Wisconsin–Madison, Madison, WI, USA, ²School of Mathematical and Physical Sciences and Research Centre in Astronomy, Astrophysics & Astrophotonics, Macquarie University, Sydney, Australia, ³Australia Telescope National Facility, CSIRO Space & Astronomy, Epping, NSW, Australia, ⁴Department of Astronomy, Columbia University, New York, NY, USA, ⁵Institut für Physik und Astronomie, Universität Potsdam, Golm (Potsdam), Germany, ⁶National Radio Astronomy Observatory, Charlottesville, VA, USA, ⁷current: Space Telescope Science Institute, Baltimore, MD, USA, ⁸School of Natural Sciences, University of Tasmania, Hobart, TAS, Australia, ⁹Department of Astronomy, University of California, Berkeley, Berkeley, CA, USA, ¹⁰current: Department of Pharmacology, College of Veterinary Medicine, Cornell University, Ithaca, NY, USA, ¹¹Research School of Astronomy & Astrophysics, The Australian National University, Canberra, ACT, Australia, ¹²Department of Astronomy, University of Illinois, Urbana, IL, USA and ¹³Deceased

Abstract

The Magellanic Stream (MS), a tail of diffuse gas formed from tidal and ram pressure interactions between the Small and Large Magellanic Clouds (SMC and LMC) and the Halo of the Milky Way, is primarily composed of neutral atomic hydrogen (HI). The deficiency of dust and the diffuse nature of the present gas make molecular formation rare and difficult, but if present, could lead to regions potentially suitable for star formation, thereby allowing us to probe conditions of star formation similar to those at high redshifts. We search for HCO⁺, HCN, HNC, and C₂H using the highest sensitivity observations of molecular absorption data from the Atacama Large Millimeter Array (ALMA) to trace these regions, comparing with HI archival data from the Galactic Arecibo L-Band Feed Array (GALFA) HI Survey and the Galactic All Sky Survey (GASS) to compare these environments in the MS to the HI column density threshold for molecular formation in the Milky Way. We also compare the line of sight locations with confirmed locations of stars, molecular hydrogen, and OI detections, though at higher sensitivities than the observations presented here.

We find no detections to a 3 σ significance, despite four sightlines having column densities surpassing the threshold for molecular formation in the diffuse regions of the Milky Way. Here we present our calculations for the upper limits of the column densities of each of these molecular absorption lines, ranging from 3×10^{10} to 1×10^{13} cm⁻². The non-detection of HCO⁺ suggests that at least one of the following is true: (i) $X_{\text{HCO}^+, \text{MS}}$ is significantly lower than the Milky Way value; (ii) that the widespread diffuse molecular gas observed by Rybarczyk (2022b, ApJ, 928, 79) in the Milky Way's diffuse interstellar medium (ISM) does not have a direct analogue in the MS; (iii) the HI-to-H₂ transition occurs in the MS at a higher surface density in the MS than in the LMC or SMC; or (iv) molecular gas exists in the MS, but only in small, dense clumps.

Keywords: ISM: molecules; radio lines: ISM; submillimetre: ISM; (galaxies:) Magellanic Clouds

(Received 12 June 2024; revised 14 September 2024; accepted 13 October 2024)

1. Introduction

The Magellanic Stream (MS) is a tail of diffuse neutral atomic hydrogen (HI) that formed from tidal and ram pressure interactions of the Small and Large Magellanic Clouds (SMC and LMC) with each other and with the Milky Way. At a metallicity of approximately 10% of the solar value (Fox et al. 2013), the MS is far less chemically enriched than the Milky Way or the LMC (45–50% solar), though comparable with the SMC (10–20% solar, Rolleston, Trundle, & Dufton 2002; Fox et al. 2013). While the part of the MS

close to the Clouds has an estimated distance of 50–65 kpc, (Keller & Wood 2006), distance to the tip of the Stream is observationally not well constrained and ranges from 20 (McClure-Griffiths et al. 2008; Casetti-Dinescu et al. 2014) to 100 kpc (Chandra et al. 2023). Other simulations suggest further distances up to 100 kpc (Besla et al. 2010; Lucchini, D'Onghia, & Fox 2021) as well.

To understand the evolution of the interstellar medium (ISM) and the process of star formation, it is important to examine a variety of interstellar environments. A necessary condition for star formation is dense, cold gas, in which self-gravity is able to overcome thermal, turbulent, and magnetic pressures. This gas is usually rich with molecules, particularly molecular hydrogen (H₂). Due to the MS's low metallicity and extended, highly diffuse nature, it offers an extremely different laboratory for studying the early stages of molecule formation (and potentially star formation, e.g. Price-Whelan et al. 2019) than the chemically enriched,

Corresponding author: Lucille Steffes; Email: ljesteffes@arizona.edu

Cite this article: Steffes Lucille, Rybarczyk DR, Stanimirović S, Dawson J. R., Putman M, Richter P, Gallagher III J, Liszt H, Murray C, Dickey JM, Heiles C, Hernandez A, Lindner R, Liu Y, McClure-Griffiths NM, Wong T and Savage B. (2024) A search for 3-mm molecular absorption line transitions in the magellanic stream. *Publications of the Astronomical Society of Australia* 41, e094, 1–10. <https://doi.org/10.1017/pasa.2024.95>

cold, dense, molecular clouds in the plane of the Milky Way. While the MS is the product of tidal and ram-pressure stripping and not a direct analogue for sites of primordial star formation, it nevertheless provides a nearby laboratory to study gas in some of the conditions that would have been present at higher redshifts (Hammer *et al.* 2015; Murray *et al.* 2015; Wang *et al.* 2019; Galametz *et al.* 2020).

The MS has been extensively imaged in HI (e.g. Putman *et al.* 2003). The HI observations of the tip of the MS, the region farthest away from the MCs (Stanimirović *et al.* 2008; Nidever *et al.* 2010), revealed several long filaments, demonstrating that the MS is very extended and with significant small-scale HI structure. The wealth of observational data (e.g. Weiner & Williams 1996; Fox *et al.* 2014; For *et al.* 2014; Kim, Zheng, & Putman 2024) suggests that the MS has a complex multi-phase structure that spans a large range in gas densities and ionisation conditions. About 15% of hydrogen clouds in the sample of Stanimirović *et al.* (2008) have velocity profiles which suggest two temperature components (one cooler at $< 2\,000$ K, and one warmer at $< 13\,000$ K). As summarised in Stanimirović & Gallagher (2010), the existence of the multi-phase medium in the MS, embedded in the ambient hot (10^6 K) Galactic halo gas, is surprising considering Stream's low metallicity, interstellar radiation field, and relevant heating and cooling rates (Wolfire *et al.* 1995; Sternberg, McKee, & Wolfire 2002). Even more surprisingly, Matthews *et al.* (2009) detected the first HI absorption lines against radio background sources located behind the MS. The two detected absorption features suggest temperatures of the absorbing clouds of 70–80 K, and hydrogen column densities of $2 \times 10^{20} \text{ cm}^{-2}$. Dempsey *et al.* (2020) searched for HI absorption in the far outskirts of the SMC – where the metallicities are similar to those in the MS (the SMC is thought to be the origin of much of the MS gas; D'Onghia & Fox 2016, and references therein) – and detected cold HI with high confidence in two out of five positions. They estimated cold HI properties as having spin temperature ~ 100 K and column density of $(6 - 16) \times 10^{20} \text{ cm}^{-2}$.

Remarkably, molecular hydrogen (H_2) has also been detected within the MS, measured through UV absorption towards the Seyfert galaxy NGC 3783 (Sembach *et al.* 2001; Wakker 2006; Richter *et al.* 2013) and towards the quasar Fairall 9 (Richter *et al.* 2001; Wakker 2006; Richter *et al.* 2018), in diffuse environments with the HI column density $< 10^{20} \text{ cm}^{-2}$. These observations suggest H_2 column densities $N(\text{H}_2) \sim 10^{18} \text{ cm}^{-2}$ and excitation temperatures of ~ 100 K. Lehner (2002) also detected more diffuse H_2 in the direction of the Magellanic Bridge, located between the SMC and the LMC, with $N(\text{H}_2) = 2.7 \times 10^{15} \text{ cm}^{-2}$. Together, these observations indicate that molecular hydrogen can form and survive in the diffuse environments that exist in the MS and the Bridge, far from the main bodies of the SMC and LMC.

While the Magellanic Bridge contains young stars (Irwin, Kunkel, & Demers 1985), numerous stellar searches in the MS were unsuccessful (e.g. Mathewson *et al.* 1979). Only very recently, Chandra *et al.* (2023) identified 13 stars that are likely located in the MS at a distance of 60–120 kpc. Some of those 13 stars are metal-rich and belong to the recently formed tidal counterpart to the MS, but other stars are metal-poor and possibly originated from the SMC outskirts during an earlier interaction between the Clouds. Zaritsky *et al.* (2020) also detected 15 stars of SMC metallicity with velocities of the MS likely formed by a tidal interaction of the MS with other compact clouds in the outer edges of the MW. Following the star formation models, we would expect that

molecular gas can form and survive in the MS if some of star formation has indeed occurred there.

Previous direct detections of H_2 in the MS have been valuable for characterising molecule formation in this extreme environment, but these measurements have been extremely rare because molecular hydrogen lacks a permanent electric dipole moment, making it extremely difficult to detect in diffuse environments such as the MS. Instead, observations from other molecular species – which are much easier to detect in emission and absorption – are most often used to trace the molecular content of the gas in these environments. While carbon monoxide (CO) – the most common tracer of molecular gas in galaxies – has been detected in emission in several positions in the Magellanic Bridge (Muller, Staveley-Smith, & Zealey 2003; Mizuno *et al.* 2006), no detections of CO emission exist for the MS. Most metallicity estimates suggest that the MS was formed out of the SMC gas, however metallicity variations along the MS suggest some mixing of the SMC/LMC gas (Fox *et al.* 2013; Richter *et al.* 2013). Several studies (e.g. Richter *et al.* 2013) suggest that the MS likely has a clumpy but widespread diffuse molecular phase that is enabled by efficient H_2 self-shielding and the absence of local UV sources (Fox 2005).

In the Milky Way, observations of the molecule HCO^+ in absorption are commonly used to trace diffuse molecular gas. HCO^+ is readily detected in absorption in directions with $A_V \gtrsim 0.25$ mag (e.g. Lucas & Liszt 1996; Rybarczyk *et al.* 2022b), evidently forming under similar conditions to the HI-to- H_2 transition. Moreover, HCO^+ absorption is regularly detected in directions where CO emission is undetected (Lucas & Liszt 1996; Liszt & Lucas 2000; Rybarczyk *et al.* 2022b). This suggests that a search for HCO^+ in absorption is among the best approaches for detecting molecular gas in the diffuse environment of MS. Indeed, Murray *et al.* (2015) reported a tentative detection of HCO^+ absorption in the Magellanic system outside of the LMC and SMC, in the low density environment of the Magellanic Bridge.

In this study, we have obtained the most sensitive observations to date of molecular absorption from key molecular species, including HCO^+ , in the MS using the the Atacama Large Millimeter/submillimeter Array (ALMA). In Section 2, we discuss the observations for each of the four molecular lines, HCO^+ , HCN, HNC, and C_2H at 10 pointings in the MS. In Section 3, we present the upper limits on the optical depths (τ) and the column densities of the four molecular species for each line of sight. In Section 4.1, we examine the position of each line of sight relative to the SMC and LMC to contextualise the column density limits presented in Section 3. We also search for possible correlations between the location conditions and the upper limits of the optical depths and column densities of different molecular species. In Section 4.2, we discuss what our observations imply for the molecular fraction in the Stream.

2. Observations

2.1. Molecular absorption measurements from ALMA

We searched for absorption by the $J = 1 - 0$ transitions of HCN (including three hyperfine lines at 88.6304–88.6339 GHz), HCO^+ (89.1890 GHz), and HNC (90.6336 GHz), and the $N = 1 - 0$ transition of C_2H (including two hyperfine lines at 87.3169 GHz and 87.3286 GHz) using ALMA Band 3 observations towards 14 background radio continuum sources (project code 2013.1.00700.S, ALMA Cycle 2). Observations were obtained between May 2015

Table 1. Summary of observations. For each source (column 1), we list the celestial coordinates (columns 2 and 3), the Magellanic Stream coordinates (columns 4 and 5), the flux density at 89 GHz (column 6), the optical depth sensitivity for HI absorption using ATCA (Column 7), and the optical depth sensitivity in the final spectra achieved for each of the four molecular transitions observed with ALMA (columns 8–11).

Source	$\alpha(^{\circ})$	$\delta(^{\circ})$	l_{MS}	b_{MS}	F_{89} (Jy)	σ_{τ,HCO^+}	$\sigma_{\tau,HCN}$	$\sigma_{\tau,HNC}$	σ_{τ,C_2H}
2331+073	353.553	7.608	-96.29	1.62	0.4683	0.023	0.021	0.023	0.020
J2230+114	338.152	11.731	-105.22	-11.37	3.014	0.004	0.004	0.004	0.004
J0635-7516	98.944	-75.271	4.87	-3.51	1.264	0.008	0.008	0.009	0.008
2355-534	359.472	-53.187	-36.28	-11.13	0.9927	0.010	0.010	0.010	0.010
J1058-8003	164.680	-80.065	11.36	-15.87	1.4230	0.017	0.010	0.016	0.014
J0454-8101	72.523	-81.017	-0.67	-8.98	2.0043	0.009	0.008	0.008	0.007
2345-167	357.011	-16.520	-72.27	-2.50	3.0402	0.005	0.005	0.005	0.004
J0049-4457	12.319	-44.953	-41.12	-0.42	0.02834	0.034	0.040	0.038	0.039
J0253-5441	43.372	-54.698	-21.40	9.58	1.1720	0.012	0.010	0.020	0.011
2326-477	352.324	-47.505	-42.99	-14.32	0.71428	0.019	0.018	0.017	0.015

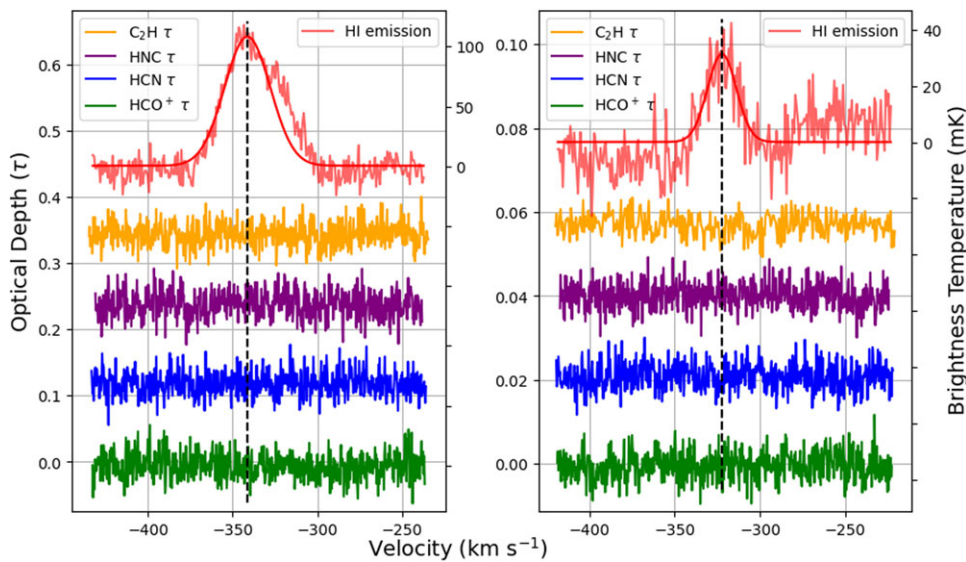


Figure 1. The optical depth spectra for the sources 2331+073 (left) and J2230+114 (right) with the corresponding HI brightness temperature spectra from the GALFA-HI survey.

and September 2015. On-source integration times ranged from 5–10 min.

Three background sources – NGC3783, NGC7714, and NGC7469 – were chosen because they had complementary UV observations. Unfortunately, all three sources were excluded from our analysis because their continuum flux densities were too low to be able to detect absorption (0.003, 0.002, and 0.003 Jy, respectively). We chose the remaining ten background sources based on their positions behind the MS and their high continuum flux densities. Table 1 lists the positions and 89 GHz flux densities of all ten sources included in our analysis. The velocity resolutions of the final absorption-line spectra ranged from 0.303 to 0.315 km s⁻¹.

The calibration and imaging for these sources were straightforward, and the ALMA pipeline products were essentially science-ready. To obtain the most accurate estimates of the continuum flux densities, though, we reran the ALMA pipeline without continuum subtraction for all of our observations. Towards each background source, we then extracted the absorption spectrum,

$$e^{-\tau(\nu)} = \frac{I(\nu)}{I_0(\nu)}, \tag{1}$$

where $\tau(\nu)$ is the optical depth, $I(\nu)$ is the observed intensity, and $I_0(\nu)$ is the continuum emission of the background source. All three quantities are functions of frequency (here we convert to radial velocity, ν). For each molecular line, we selected the pixel with the brightest continuum flux density and extracted the spectrum ($I(\nu)$ in Equation 1) from the spectral cube at that pixel. To model the continuum ($I_0(\nu)$ in Equation 1), we fit a constant value using the spectral channels where HI is not seen in emission, and therefore no molecular absorption is expected (e.g. Rybarczyk et al. 2022b). We chose to fit a constant because the continuum was nearly flat across each of the 58.50 MHz spectral windows.

In Figs. 1 and 2, we show the optical depth spectra, $\tau(\nu)$, measured towards each background source. From bottom to top, we plot the optical depth spectra of HCO⁺ (green), HCN (blue), HNC (purple), C₂H (yellow).

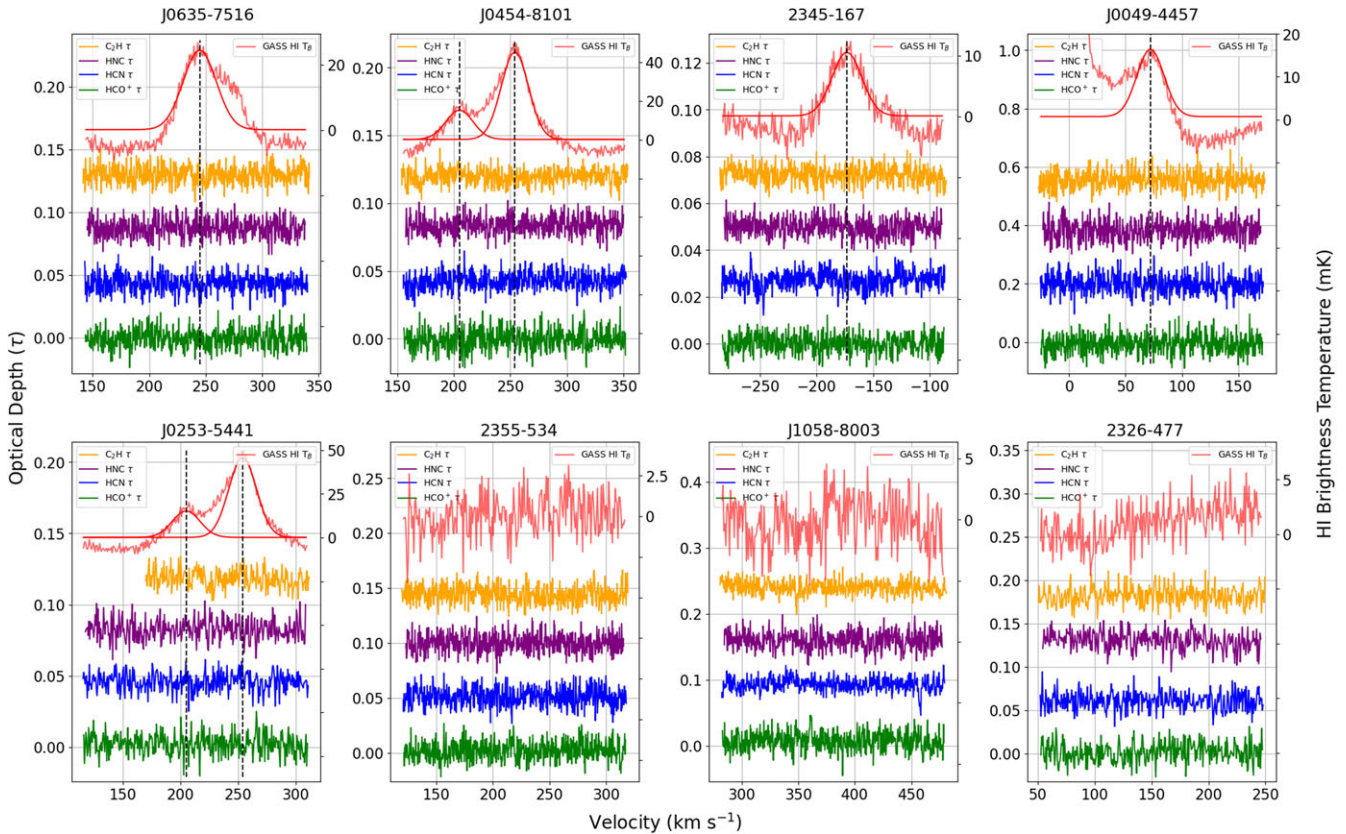


Figure 2. The optical depth spectra for the sources J0635-7516, J0454-8101, 2345-167, J0049-4457, J0253-5441, 2355-534, J1058-8003, and 2326-477 with their corresponding HI brightness temperature spectra from GASS.

2.2. Complementary HI measurements

In Figs. 1 and 2, we show the HI emission spectrum (red, top) alongside the optical depth spectra measured in the direction of each background source. Fig. 1 uses HI emission spectra measured by the Galactic Arecibo L-band Feed Array HI (GALFA-HI) Survey (Peek et al. 2011, 2018). The HI spectra in Fig. 2 come from the Galactic All Sky Survey (GASS, McClure-Griffiths et al. 2009) and the HI4PI survey (HI4PI Collaboration et al. 2016). The $1\sigma_{rms}$ noise level is 43, 55, and 60–140 mK for the GASS, HI4PI, and GALFA-HI surveys, respectively (HI4PI Collaboration et al. 2016; McClure-Griffiths et al. 2009; Peek et al. 2018), corresponding to $1\sigma_{rms} N(\text{HI})$ sensitivities $\sim 2.3 \times 10^{18} \text{cm}^{-2}$, $2.5 \times 10^{18} \text{cm}^{-2}$, and $6.5 \times 10^{18} \text{cm}^{-2}$, assuming a FWHM of 20, 30, and 20 km s^{-1} , respectively. For each sightline, we fit a Gaussian function to the main emission feature. The centroid velocity of the fit is shown with the black dashed vertical lines in Figs. 1 and 2 to emphasise at which velocities molecular absorption lines would be expected if present.

Molecular gas forms from relatively cold and dense HI; if cold molecular gas were present in any of these directions, we would also expect cold HI to be present and potentially detectable in absorption (e.g. Stanimirović et al. 2014; Nguyen et al. 2019; Rybarczyk et al. 2022b; Park et al. 2023; Hafner et al. 2023). Moreover, HI absorption observations would probe a similar physical scale to our pencil-beam molecular absorption line spectra, whereas HI emission observations probe a much larger physical scale. Murray et al. (2015) observed several of the same sources

observed in this study in several wavelengths including HI absorption. These yielded all non-detections for the observed sources. Because we detect no HI gas in absorption, our assumption made in Section 3 is valid and we derive all HI column densities and velocities from the HI emission spectra.

3. Limits on the molecular column densities in the MS

We do not detect HCO^+ , C_2H , HCN , or HNC absorption in the direction of any of the 10 background sources listed in Table 1 at a level of 3σ . In Table 1, we list the 1σ noise in $\tau(\nu)$ for velocity channels of width $\sim 0.3 \text{ km s}^{-1}$ for each transition and each line of sight. Our sensitivity is comparable to that achieved by Rybarczyk et al. (2022a), who detected HCO^+ absorption in 10 diffuse sightlines through the Milky Way. If we assume a conversion factor $X_{\text{HCO}^+} \sim \text{few} \times 10^{-9}$ as suggested by Millar & Herbst (1990) for both the SMC and LMC, our upper limit on the H_2 column density is $\sim 10^{19} \text{cm}^{-2}$ (although see discussion of HCO^+ abundance in Section 4.2).

To estimate upper limits to the column densities of HCO^+ , HCN , HNC , and C_2H we make several assumptions about the nature of a molecular line detection in this environment. The column density, N , of a molecular species is related to the optical depth, $\tau(\nu)$, by

$$N = C(T_{\text{ex}}) \int \tau(\nu) d\nu, \quad (2)$$

Table 2. Conversion factors from integrated optical depth to column density ($C(T_{\text{ex}})$ in Equation 2) for the transitions observed in this work, assuming $T_{\text{ex}} = 2.725$ K (e.g. Godard et al. 2010; Luo et al. 2020).

Species	$C(T_{\text{ex}}) = N / \int \tau dv$ ($\text{cm}^{-2} / \text{km s}^{-1}$)
C ₂ H	4.34×10^{13}
HCN	1.91×10^{12}
HCO ⁺	1.11×10^{12}
HNC	1.78×10^{12}

where C depends on the the excitation temperature, T_{ex} , and the physical properties of the observed transition (e.g. Draine 2011). We assume an excitation temperature equal to the temperature of the CMB, 2.725 K, for all lines, as is typically assumed in diffuse environments (e.g. Lucas & Liszt 1996; 2000; Liszt & Lucas 2001) and has been confirmed in some diffuse directions for HCO⁺ (Godard et al. 2010; Luo et al. 2020). Values for $C(2.725$ K) are listed in Table 2. We also assume that any molecular absorption lines are Gaussian, with peak optical depth τ_0 and full width at half maximum (FWHM) Δv_0 . Then, the column density is $N = C(T_{\text{ex}}) \times 1.064 \times \tau_0 \times \Delta v_0$. We assume a minimum FWHM of 2 km s^{-1} (e.g. Lucas & Liszt 1996; Godard et al. 2010; Rybarczyk et al. 2022a). Since we find only non-detections, in Table 3 we report upper limits to the molecular column densities using $\tau_0 = 3\sigma_\tau$.

We also compare these molecular column density upper limits with the HI column densities and surface densities (Table 3). We find the column densities of the HI using the integrated intensities averaged over $20''$ when using the GALFA-HI data and $44''$ when using the GASS data to account for diffuse larger structures in that region. The sizes of the areas differed between the two HI surveys because the angular resolution was far improved in the GALFA-HI survey compared to the GASS survey, which allowed the HI emission in the MS to be resolved on smaller angular scales. However because the intensities were averaged, we find minimal differences in the outcomes. These values are then multiplied by a scale factor of $1.823 \times 10^{18} \text{ cm}^{-2} / (\text{K km s}^{-1})$ (Murray et al. 2018). This assumes an optically thin environment, so these represent lower limits of the HI column densities. We then use a scale factor of 0.8×10^{-20} to convert between the HI column densities, $N(\text{HI})$, and the HI surface densities, $\Sigma(\text{HI})(M_\odot \text{pc}^{-2})$ (Roman-Duval et al. 2014).

We compare these results with those of Murray et al. (2015), who found a tentative detection of HCO⁺ towards J0454-8101 with a peak τ of 0.10 ± 0.02 with $\sigma_\tau = 0.026$ per 0.8 km s^{-1} velocity channels using the Australia Telescope Compact Array (ATCA). For HCO⁺ our value at J0454-8101 was $\sigma_\tau = 0.009$, which would make our 3σ upper limit equal to $\tau = 0.027$. We are unable to reproduce the results of Murray et al. (2015) here. The tentative detections from Murray et al. (2015) could be a result of radio frequency interference (RFI) contamination. The location of ALMA should be less susceptible to RFI contamination than ATCA, and our observations have both a higher sensitivity and an increased bandpass stability.

Finally, in an effort to improve the signal-to-noise ratio in our molecular absorption spectra, we stack all 10 spectra for each molecular absorption line to create a weighted mean spectrum (Fig. 3). The spectra are weighted by the inverse square of the standard deviation of individual spectra. When stacking, all

of the composite spectra are shifted in velocity so that 0 km s^{-1} in each stacked spectrum aligns with the peak in the HI emission spectrum.^a The optical depth sensitivities for each of the stacked molecular absorption spectra are listed in Table 4. Stacking improves the signal to noise ratio by a factor of 1.5 – 10 compared to the individual spectra shown in Figs. 1 and 2. Even with the reduced noise in the stacked spectra, though, we still do not detect molecular absorption at a level 3σ in any of the four lines. Upper limits to the molecular column densities in the stacked spectra are listed in Table 4.

4. Discussion

4.1. Spatial distribution of molecular upper limits across the Magellanic Stream

In Fig. 4, we show the locations of our background sources across the MS, using a colour bar to indicate the upper limits of the column density of each molecular line. The background of Fig. 4 shows the column density of the high velocity ($|v_{\text{LSR}}| < 450 \text{ km s}^{-1}$, $v_{\text{dev}} = 70 \text{ km s}^{-1}$) HI emission in the MS and Leading Arm from the LAB (Leiden/Argentine/Bonn) survey (Westmeier 2018), calculated using the HI4PI all sky survey (HI4PI Collaboration et al. 2016). The HI column density is shown using the Magellanic Stream Coordinate System (Nidever, Majewski, & Butler Burton 2008).

We transformed the coordinates of each of the background sources to the Magellanic Stream Coordinate System to emphasise the MS and Leading Arm in the HI4PI data. This was accomplished following the equations first introduced by Wakker (2001) and Nidever et al. (2008),

$$\tan(\lambda - \lambda_0) = \frac{\sin(b) \sin(\varepsilon) + \cos(b) \cos(\varepsilon) \sin(l - l_0)}{\cos(b) \cos(l - l_0)} \quad (3)$$

$$\sin(\beta) = \sin(b) \cos(\varepsilon) - \cos(b) \sin(\varepsilon) \sin(l - l_0), \quad (4)$$

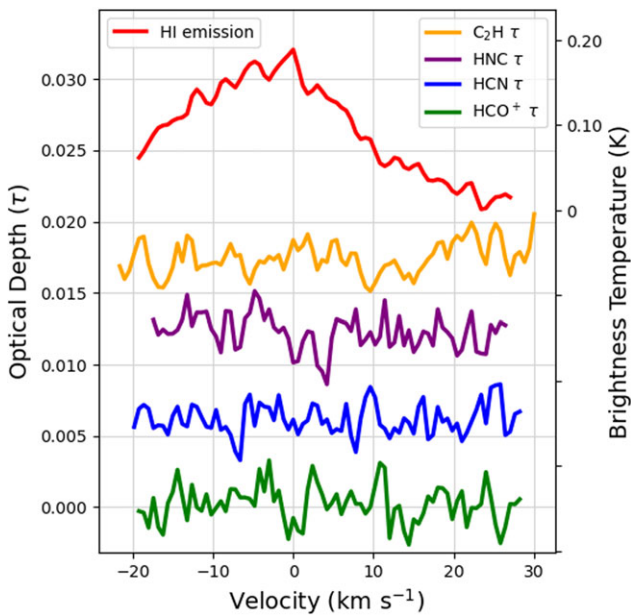
where l and b are the Galactic latitude and longitude values, which return λ and β , the Magellanic longitude and latitude values. In these equations, $l_0 = 278.5^\circ$, $\lambda_0 = 32.861^\circ$, and $\varepsilon = 97.5^\circ$ (Nidever et al. 2008).

As shown in Fig. 4, we probe a range of HI column density environments. Two sources probe gas in the outskirts of the Magellanic Clouds with higher HI column densities ($2 \times 10^{19} \text{ cm}^{-2}$) and less filamentary and dispersed gas structures. Three sources probe the Leading Arm (gas on the opposite side of the Stream). At one of these sources (J1058-8003), we do not detect HI and therefore provide an upper limit to the column density as seen in Table 3. The remaining seven sources are in the direction of the Stream with varied column densities ranging from $4 \times 10^{17} - 3 \times 10^{19} \text{ cm}^{-2}$, though at two of these sources (2345-167 and 2326-477) we do not detect HI emission. Upper limits for the column densities can again be found in Table 3. Our sensitivity is roughly uniform across our sample. For most sources, we find $N(\text{HCO}^+) \lesssim \text{few} \times 10^{10} \text{ cm}^{-2}$, both around the MCs and in the leading arm of the MS.

^aIdeally, we would align the spectra along the velocity of peak HI absorption, since we expect molecular absorption to be associated with cold HI. Because we do not detect HI absorption in these directions, though, we use the HI emission instead. Figs. 1 and 2 show that the HI emission spectra are quite simple in these directions, with only one or two components.

Table 3. HI column density and surface density and upper limits (3σ) of the column densities of HCO^+ , HCN, HNC, and C_2H for each line of sight in our sample.

Position	$N(\text{HI})$ 10^{17} cm^{-2}	$\Sigma(\text{HI})$ $M_{\odot} \text{ pc}^{-2}$	$N(\text{HCO}^+)$ 10^{11} cm^{-2}	$N(\text{HCN})$ 10^{11} cm^{-2}	$N(\text{HNC})$ 10^{11} cm^{-2}	$N(\text{C}_2\text{H})$ 10^{12} cm^{-2}
2331+073	180.5	0.14	< 1.636	< 2.504	< 2.490	< 5.428
J2230+114	45.5	0.036	< 0.290	< 0.442	< 0.411	< 1.029
J0635-7516	140.0	0.11	< 0.587	< 1.006	< 1.051	< 2.387
2355-534	4.1	0.0033	< 0.725	< 1.185	< 1.155	< 2.725
J1058-8003	< 0.3	< 0.0003	< 1.211	< 1.242	< 1.778	< 3.628
J0454-8101	190.6	0.15	< 0.625	< 0.983	< 0.863	< 1.874
2345-167	< 38.2	< 0.031	< 0.327	< 0.565	< 0.522	< 1.367
J0049-4457	30.7	0.025	< 2.392	< 4.999	< 4.330	< 10.774
J0253-5441	306.6	0.25	< 0.843	< 1.374	< 1.461	< 2.969
2326-477	< 30.6	< 0.025	< 1.265	< 2.035	< 2.040	< 4.792

**Figure 3.** The smoothed and stacked spectra for each of the molecular species and the HI emission spectrum from GASS and GALFA.

Several previous studies have detected H_2 using UV spectroscopy in the direction of the MS (Sembach et al. 2001; Richter et al. 2001; Wakker 2006; Richter et al. 2013, 2018) and Magellanic Bridge (Lehner 2002). Sembach et al. (2001), Wakker (2006), and Richter et al. (2018) detected H_2 and other species towards the MS Leading Arm, while Richter et al. (2001), Wakker (2006), and Richter et al. (2013) detected H_2 and other species towards the MS. In both directions, best estimates for the H_2 column densities are $N(\text{H}_2) \sim 10^{18} \text{ cm}^{-2}$, with $f_{\text{mol}} = 2n(\text{H}_2)/n_{\text{H}} \approx 0.01\text{--}0.04$. H_2 has also been detected in the Magellanic Bridge (Lehner 2002), but with relatively lower column density, $N(\text{H}_2) = 2.7 \times 10^{15} \text{ cm}^{-2}$, and lower molecular fraction, $f_{\text{mol}} \approx 10^{-5}\text{--}10^{-4}$. In Section 4.2 below, we discuss our non-detections in the context of these previous results.

Recently, several studies claimed the detection of stars along and around the MS. Chandra et al. (2023) detected 13 stars, of ages 4–10 Gyr, trailing the past orbits of the Clouds. Based on

Table 4. Upper limits (3σ) of the column densities for the stacked spectra of HCO^+ , HCN, HNC, and C_2H .

Molecular species	Column density (cm^{-2})	σ_{τ}
HCO^+	< 9.257×10^9	0.0013
HCN	< 1.644×10^{10}	0.0012
HNC	< 1.226×10^{10}	0.0010
C_2H	< 3.478×10^{11}	0.0012
HI	8.100×10^{18}	–

kinematics and metallicity these are high-confidence members of the MS. These stars, which we show in Fig. 5, have two populations: about half of the stars form a higher-metallicity population that tracks the HI well, and the rest of the stars form a diffuse, lower-metallicity population that is offset from the HI by about 20 degrees. The higher-metallicity stars were most likely formed in the LMC disc and were stripped at the same time as the HI gas. However, if formed in-situ, as was suggested for 1–4 Gyr-old stars discovered in the Milky Way Halo (Price-Whelan et al. 2019), thought to have formed during the last interaction of the Leading Arm, these stars in the MS would need cold and dense molecular gas to form. The origin of the lower-metallicity stars is harder to constrain, with one idea being that those stars were thrown out of the SMC outskirts during past interactions between the Clouds. If some of recently detected stars were formed in-situ, Price-Whelan et al. (2019) proposes this to have occurred with tidally stripped gas interacting with Milky Way halo gas during recent low-mass mergers. During these interactions, the turbulence of the infalling gas could have created cold and dense regions where some star formation may have occurred (see Mac Low & Klessen 2004, and references therein); molecular gas would also be formed in this process. The existence of stars in the MS therefore suggests the possibility of the presence of molecular gas, which we constrain here.

Using the Cosmic Origins Spectrograph (COS) on the Hubble Space Telescope, recent studies observed OI in the Magellanic Corona, surrounding the Magellanic Clouds and into the MS (Krishnarao et al. 2022). These 12 detections were found to be consistent with tidally stripped gas from the Magellanic Stream rather than originating in the more higher temperature (10^6 K)

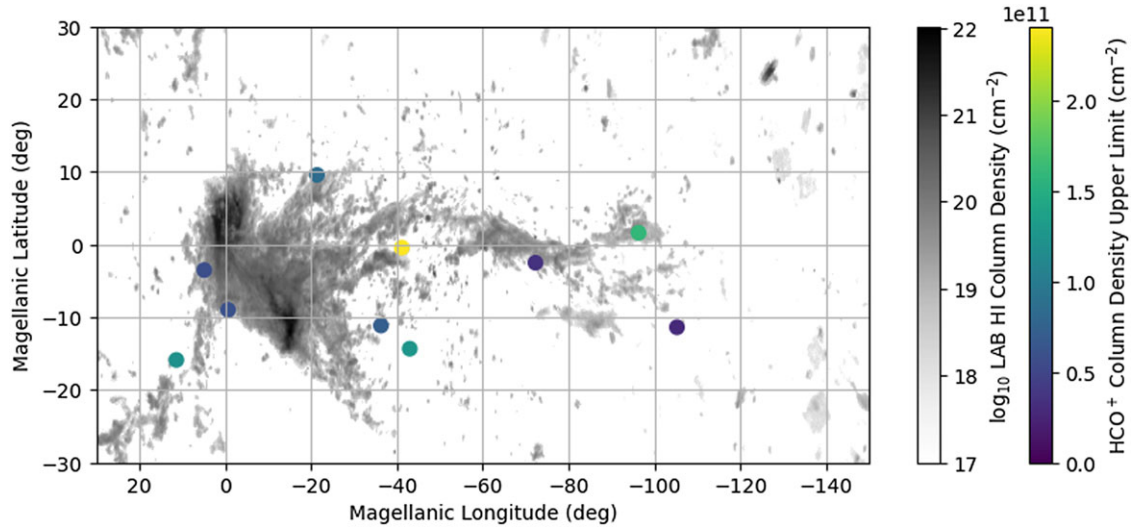


Figure 4. The Upper Limits of the Column Densities of HCO⁺ plotted against the HI column density map of the high velocity components ($\pm 100 \text{ km s}^{-1}$) of the Magellanic Stream using the Magellanic Stream Coordinate System. The image is from the LAB High Velocity Cloud Sky Survey and has angular resolution of 36' (Westmeier 2018).

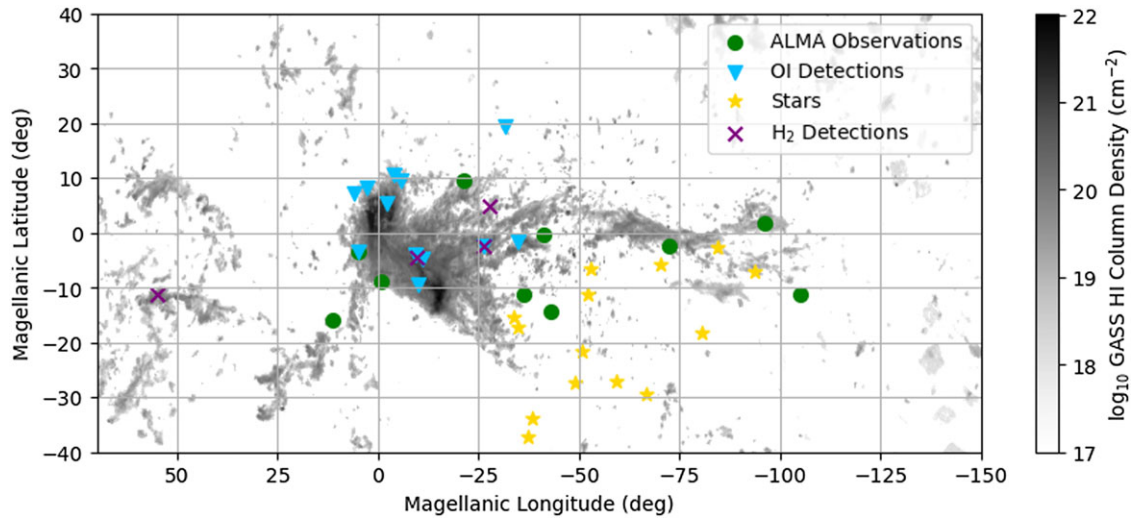


Figure 5. A spatial comparison between detections of O I (blue triangles), stars (yellow stars), H₂ (purple xs), and our observations (green circles) in the Magellanic Stream and Leading Arm, plotted in the background using data from the LAB High Velocity Cloud Sky Survey.

and highly ionised Magellanic Corona (Krishnarao et al. 2022). The other ionised species detected with COS indicated a higher correlation with LMC latitudes, suggesting origins from impacts with the LMC, while the OI correlated stronger with the MS (Krishnarao et al. 2022).

In Fig. 5, we show a spatial comparison of the sightlines observed in this work to directions with previously detected H₂, OI, and stars. From this figure, we see that while some of the observed targets probe similar environments, many do not. The majority of the OI detections (Krishnarao et al. 2022) probe regions closer to the Magellanic Clouds and the Magellanic Corona, which shows higher HI column densities and in several cases correspond spatially with detections of H₂ (Richter et al. 2001; Sembach et al. 2001; Lehner 2002). Most of the detected stars (Chandra et al. 2023) do not trace similar regions of the MS compared to our observations, or any of the detections of OI or H₂.

4.2. Constraints on the molecular fraction

In the diffuse ISM of the Milky Way, the abundance of HCO⁺ with respect to H₂ is roughly constant, with only a limited scatter, $N(\text{HCO}^+)/N(\text{H}_2) = 3 \times 10^{-9} \pm 0.2 \text{ dex}$ (Gerin et al. 2019; Liszt & Gerin 2023). If HCO⁺ is a similarly good tracer of H₂ in the MS, then we can constrain $N(\text{H}_2)$ and set an upper limit on the molecular fraction of the gas in our MS sightlines,

$$f_{\text{mol}} = \frac{2N(\text{HCO}^+)/X_{\text{HCO}^+, \text{MS}}}{N(\text{HI}) + 2N(\text{HCO}^+)/X_{\text{HCO}^+, \text{MS}}} = \left(1 + \frac{N(\text{HI})X_{\text{HCO}^+, \text{MS}}}{2N(\text{HCO}^+)}\right)^{-1}, \tag{5}$$

where $X_{\text{HCO}^+, \text{MS}} = N(\text{HCO}^+)/N(\text{H}_2)$ in the MS. We note that our estimates for $N(\text{HCO}^+)$ come from pencil-beam absorption spectra, whereas our estimates for $N(\text{HI})$ come from emission spectra with much larger beam sizes. Ideally, we would compare

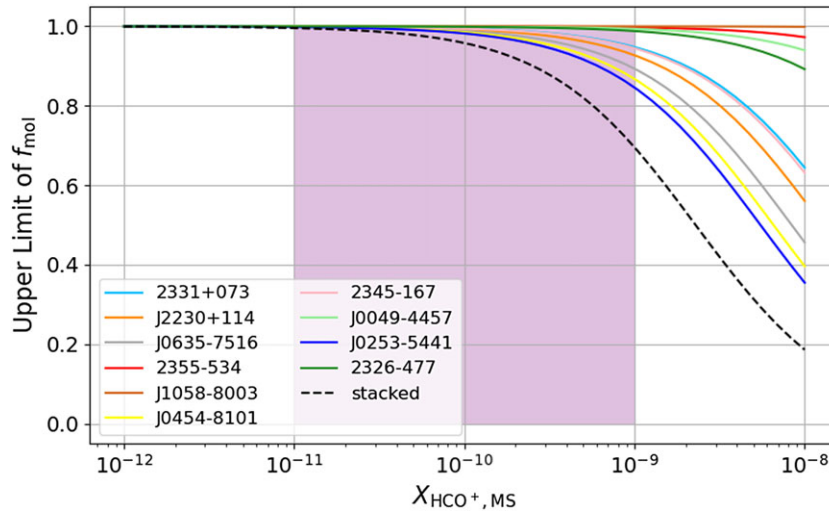


Figure 6. The upper limit on f_{mol} as a function of $X_{\text{HCO}^+, \text{MS}}$ (Equation 5) for each source.

our molecular absorption observations to HI absorption observations in order to probe similar physical scales. However, because we do not detect HI in absorption, we use the emission observations to estimate the total column density of the atomic hydrogen. Equation (5) implicitly assumes that $N(\text{HI})$ and $N(\text{H}_2)$ are probing the same environment, so our non-uniform approach allows us only to make an approximate measurement of the relationship between f_{mol} and $X_{\text{HCO}^+, \text{MS}}$.

In Fig. 6, we show what our measurements of $N(\text{HI})$ and $N(\text{HCO}^+)$ imply for f_{mol} for a range of possible $X_{\text{HCO}^+, \text{MS}}$. To properly interpret our results, we need some reasonable estimate of $X_{\text{HCO}^+, \text{MS}}$. Millar & Herbst (1990) suggest an abundance of $X_{\text{HCO}^+} \sim \text{few} \times 10^{-9}$ for both the SMC and LMC, similar to that observed in the Milky Way's diffuse ISM, although their analysis focuses on dark clouds which may be much denser than the diffuse environments of the Stream and therefore have a different X_{HCO^+} (e.g. Panessa et al. 2023). We further note that Millar & Herbst (1990) estimates are probably inflated due to the low estimate of the H_3^+ dissociative recombination rate (see summary by Larsson, McCall, & Orel 2008, and references therein). The MS has a lower density than dark clouds and a lower metallicity than the LMC. The relationships of X_{HCO^+} with density and with metallicity are non-linear, so it is difficult to estimate $X_{\text{HCO}^+, \text{MS}}$ from SMC and LMC analogues. If we use a PDR model (Gong, Ostriker, & Wolfire 2017) with conservative estimates for the cosmic ray ionisation rate, temperature, density, metallicity, and interstellar radiation field of gas in the MS (motivated by direct measurements or comparisons to the SMC/LMC, e.g. Fox et al. 2013; Barger et al. 2017; Dempsey et al. 2020; Kosenko & Balashev 2023), we find a range of X_{HCO^+} values between $\mathcal{O}(10^{-12})$ and $\mathcal{O}(10^{-10})$. However, the fixed abundance of HCO^+ in the Milky Way (Gerin et al. 2019; Liszt & Gerin 2023) is an empirical result whose origin remains poorly understood. This result is not predicted by equilibrium chemical models, and PDR models generally underpredict the abundance of HCO^+ in diffuse environments (e.g. Godard et al. 2010). Given these considerations, we take the range of $10^{-11} \lesssim X_{\text{HCO}^+, \text{MS}} \lesssim 10^{-9}$ to be plausible (this region is shaded in Fig. 6), but we consider an even wider range of possible $X_{\text{HCO}^+, \text{MS}}$ values in Fig. 6. Because $N(\text{HCO}^+)$ is an upper limit for each line of sight,

the curves in Fig. 6 indicate upper limits to f_{mol} as a function of $X_{\text{HCO}^+, \text{MS}}$.

If $X_{\text{HCO}^+, \text{MS}} \lesssim 10^{-10}$, our observations do not give us tight constraints on the molecular fraction beyond indicating that the gas is not fully molecular. If $10^{-10} \lesssim X_{\text{HCO}^+, \text{MS}} \lesssim 10^{-9}$, we can place only slightly better constraints on the sightlines with the highest HI column densities – in this case, the gas towards J0253-5441, J0454-8101, and J0635-7516 must be $< 90\%$ molecular, while the gas towards J2230+114 and J1058-8003 must be $< 95\%$ molecular. Despite our excellent HCO^+ optical depth sensitivity, the low column densities of the gas in the direction of our background sources mean that, for any plausible $X_{\text{HCO}^+, \text{MS}}$, we can only place weak limits on the fraction of molecular gas towards our 10 lines of sight. If we consider the stacked spectrum, where we achieve an HCO^+ optical depth sensitivity $\sigma_\tau \sim 0.001$ (Table 4), we can place somewhat more stringent limits on the molecular fraction: for $X_{\text{HCO}^+, \text{MS}} \lesssim 10^{-10}$, we can still only say that the MS gas is less than $\sim 95\%$ molecular, but for $10^{-10} \lesssim X_{\text{HCO}^+, \text{MS}} \lesssim 10^{-9}$, we find upper limits on the molecular fraction of $\sim 70\text{--}90\%$.

Previously, direct measurements of H_2 using UV absorption have placed tighter constraints on the molecular fraction in different parts of the Magellanic System. In the direction of the MS, towards the quasar Fairall 9, observations of H_2 and other neutral species suggest $f_{\text{mol}} = 0.01$ (Richter et al. 2001; Wakker 2006; Richter et al. 2013). Meanwhile, in the direction of the Leading Arm of the MS, towards the Seyfert galaxy NGC 3783, observations suggest $f_{\text{mol}} = 0.04$ (Sembach et al. 2001; Wakker 2006; Richter et al. 2013). In the Magellanic Bridge, observations suggest a lower molecular fraction, $f_{\text{mol}} = 10^{-5}\text{--}10^{-4}$ (Lehner 2002).

In Fig. 7, we show the HCO^+ column density implied by $f_{\text{mol}} = 0.04$ (Sembach et al. 2001; Wakker 2006; Richter et al. 2013) as a function of $X_{\text{HCO}^+, \text{MS}}$. Lines of different colour show the results for different HI column densities. On the right side of the plot, we show the HCO^+ optical depth (assuming a FWHM of 2 km s^{-1}) corresponding to the HCO^+ column density on the left axis. As in Fig. 6, we highlight in purple the range of $X_{\text{HCO}^+, \text{MS}}$ that we deem most plausible for the MS. We further highlight in grey the range of HCO^+ optical depths that could plausibly be detected at a level $\geq 3\sigma$ with ALMA for sources with 90 GHz flux densities

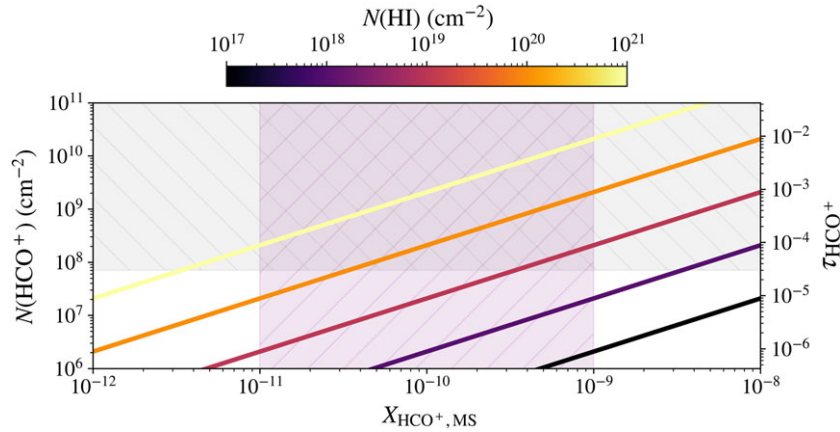


Figure 7. The HCO^+ column density (left y-axis) expected if $f_{\text{mol}} = 0.04$ in the MS (Sembach et al. 2001; Wakker 2006; Richter et al. 2013) as a function of $X_{\text{HCO}^+, \text{MS}}$. The right y-axis shows the corresponding HCO^+ optical depth (assuming a Gaussian line with 2 km s^{-1} FWHM). Lines show the results for $N(\text{HI}) = 10^{17} \text{ cm}^{-2}$, 10^{18} cm^{-2} , 10^{19} cm^{-2} , 10^{20} cm^{-2} , and 10^{21} cm^{-2} (colours correspond to the HI column density). The region highlighted in purple outlines the range of plausible $X_{\text{HCO}^+, \text{MS}}$ (Section 4.2). The region highlighted in grey indicates the range of τ_{HCO^+} that could be detected with ALMA in $\lesssim 15$ hr for the sources listed in Table 1.

listed in Table 1 (note that the flux density sensitivity needed to reach an optical depth sensitivity σ_τ is $\sigma_F = \sigma_\tau \times F$, where F is the flux density of the background source in Jy). The intersection of the purple- and grey-highlighted regions in Fig. 7 (highlighted with cross-hatching) represents the space in which we could detect HCO^+ with ALMA in $\lesssim 15$ hr if $f_{\text{mol}} = 0.04$. For any sightline with an HI column density $\gtrsim 10^{20} \text{ cm}^{-2}$, ALMA should be able to detect HCO^+ if $f_{\text{mol}} \sim 0.04$. For $10^{19} \text{ cm}^{-2} \lesssim N(\text{HI}) \lesssim 10^{20} \text{ cm}^{-2}$, we could reasonably expect to detect HCO^+ if $X_{\text{HCO}^+, \text{MS}} \gtrsim \times 10^{-10}$. It is unlikely that HCO^+ could be detected for sightlines with $N(\text{HI}) \lesssim 10^{19} \text{ cm}^{-2}$.

5. Conclusions

We have carried out the most sensitive search to date for molecular gas at millimetre wavelengths towards the MS. Despite our excellent sensitivity, we do not detect absorption from any of the four molecular species we observed – HCO^+ , HCN, HNC, and C_2H . We still do not detect absorption in any of these species when we stack the absorption spectra from our 10 sightlines, reaching an optical depth sensitivity of 10^{-3} in each of the four lines (Table 4). This includes our observations in the direction of J0454-8101 (towards the Magellanic Bridge), where Murray et al. (2015) reported a tentative detection of HCO^+ absorption. Despite our improved optical depth sensitivity ($\sigma_\tau = 0.009$ per 0.3 km s^{-1} channel, versus $\sigma_\tau = 0.026$ per 0.8 km s^{-1} channel in Murray et al. 2015); we are unable to reproduce their result.

Using complementary HI emission (McClure-Griffiths et al. 2009; Peek et al. 2011, 2018), we look at the environments in the MS where we fail to detect molecular gas (Figs. 4 and 5) and place upper limits on the fraction of hydrogen in H_2 in these environments. Over a plausible range of HCO^+ abundances in the MS, we find that the column densities are so low that, even with our excellent sensitivity, our HCO^+ column density limits only constrain the molecular fraction as $\lesssim 90\%$ in most cases (if the HCO^+ abundance is $\gtrsim 10^{-10}$, see Fig. 6). For the stacked spectrum, we can place slightly more stringent limits, with an upper limit of $f_{\text{mol}} \sim 70\text{--}95\%$ over a range of possible HCO^+ abundances. Previous estimates of the molecular fraction in the MS, derived from direct observations of H_2 and other species in UV absorption, range

from extremely low, $\sim 10^{-5}\text{--}10^{-4}$ (Lehner 2002), to more moderate, $\sim \text{few} \times 10^{-2}$ (Sembach et al. 2001; Wakker 2006; Richter et al. 2013). To be sensitive to this latter range, we estimate that an HCO^+ optical depth sensitivity of $\mathcal{O}(10^{-5})$ to $\mathcal{O}(10^{-3})$ is required (note this depends on both the HI column density and HCO^+ abundance; see Equation 5). For background sources as bright as those observed in this project, we show that ALMA would be capable of detecting such diffuse molecular gas in an observing time $\lesssim 16 \text{ hr}^b$ if the HI column density is $\gtrsim 10^{19} \text{ cm}^{-2}$ (see Fig. 7). This suggests that ALMA offers an important way to test the existence of molecular gas in the MS, though this requires considerably better sensitivity than achieved here (note that our sources were observed for ≤ 10 min in ALMA Cycle 2).

Acknowledgements. We note the passing of our scientific colleague Prof. Blair Savage on 2022 July 19 in Madison, Wisconsin. With his students, postdocs, and colleagues, Blair made seminal contributions to studies of the interstellar and intergalactic medium. His enthusiasm for studying molecular hydrogen and dust in the MS was infectious. We would like to thank Nickolas Pingel and Trey Wenger for their insight on this project and continual discussion at group meetings. We would also like to thank Scott Lucchini and Tobias Westmeier for their help in understanding the Magellanic Stream Coordinate System. This project was partially funded by a Hilldale Undergraduate Research Fellowship, awarded in 2021 by the University of Wisconsin–Madison. We would like to thank both the Undergraduate Research Scholars Program at the University of Wisconsin–Madison and the Hilldale Undergraduate Research Fellowship for helping to make this project possible. This paper makes use of the following ALMA data: ADS/JAO.ALMA#2013.1.00700.S. ALMA is a partnership of ESO (representing its member states), NSF (USA) and NINS (Japan), together with NRC (Canada), MOST and ASIAA (Taiwan), and KASI (Republic of Korea), in cooperation with the Republic of Chile. The Joint ALMA Observatory is operated by ESO, AUI/NRAO and NAOJ. The National Radio Astronomy Observatory is a facility of the National Science Foundation operated under cooperative agreement by Associated Universities, Inc.

Data availability. Not applicable.

^bSee the ALMA Sensitivity Calculator, <https://almascience.eso.org/proposing/sensitivity-calculator>.

References

- Barger, K. A., et al. 2017, *ApJ*, **851**, 110
- Besla, G., et al. 2010, *ApJL*, **721**, L97
- Casetti-Dinescu, D. I., et al. 2014, *ApJL*, **784**, L37
- Chandra, V., et al. 2023, arXiv e-prints, arXiv:2306.15719
- D’Onghia, E., & Fox, A. J. 2016, *ARA&A*, **54**, 363
- Dempsey, J., McClure-Griffiths, N. M., Jameson, K., & Buckland-Willis, F. 2020, *MNRAS*, **496**, 913
- Draine, B. T. 2011, *Physics of the Interstellar and Intergalactic Medium* HI4PI Collaboration, et al. 2016, *A&A*, **594**, A116
- For, B. Q., Staveley-Smith, L., Matthews, D., & McClure-Griffiths, N. M. 2014, *ApJ*, **792**, 43
- Fox, A. J. 2005, PhD thesis, University of Wisconsin, Madison
- Fox, A. J., et al. 2013, *Msngr* **153**, 28
- Fox, A. J., et al. 2014, *ApJ*, **787**, 147
- Galametz, M., et al. 2020, *A&A*, **643**, A63
- Gerin, M., et al. 2019, *A&A*, **622**, A26
- Godard, B., Falgarone, E., Gerin, M., Hily-Blant, P., & de Luca, M. 2010, *A&A*, **520**, A20
- Gong, M., Ostriker, E. C., & Wolfire, M. G. 2017, *ApJ*, **843**, 38
- Hafner, A., et al. 2023, *PASA*, **40**, e015
- Hammer, F., et al. 2015, *ApJ*, **813**, 2
- Irwin, M. J., Kunkel, W. E., & Demers, S. 1985, *Nature*, **318**, 160
- Keller, S. C. & Wood, P. R. 2006, *ApJ*, **642**, 834
- Kim, D. A., Zheng, Y., & Putman, M. E. 2024, arXiv e-prints, arXiv:2402.08810
- Kosenko, D. N. & Balashev, S. A. 2023, *MNRAS*, **525**, 2820
- Krishnarao, D., et al. 2022, *Nature*, **609**, 915
- Larsson, M., McCall, B. J., & Orel, A. E. 2008, *ChPhL*, **462**, 145
- Lehner, N. 2002, *ApJ*, **578**, 126
- Liszt, H., & Gerin, M. 2023, *ApJ*, **943**, 172
- Liszt, H., & Lucas, R. 2000, *A&A* **355**, 333
- Liszt, H., & Lucas, R. 2001, *A&A*, **370**, 576
- Lucas, R., & Liszt, H. 1996, *A&A* **307**, 237
- Lucas, R., & Liszt, H. S. 2000, *A&A* **358**, 1069
- Lucchini, S., D’Onghia, E., & Fox, A. J. 2021, *ApJL*, **921**, L36
- Luo, G., et al. 2020, *ApJL*, **889**, L4
- Mac Low, M.-M., & Klessen, R. S. 2004, *RvMP*, **76**, 125
- Mathewson, D. S., Ford, V. L., Schwarz, M. P., & Murray, J. D. 1979, in *The Large-Scale Characteristics of the Galaxy*, ed. W. B. Burton, Vol. **84**, 547
- Matthews, H., et al. 2009, *AJ*, **138**, 1380
- McClure-Griffiths, N. M., et al. 2008, *ApJL*, **673**, L143
- McClure-Griffiths, N. M., et al. 2009, *ApJS*, **181**, 398
- Millar, T. J., & Herbst, E. 1990, *MNRAS*, **242**, 92
- Mizuno, N., et al. 2006, *ApJL*, **643**, L107
- Muller, E., Staveley-Smith, L., & Zealey, W. J. 2003, *MNRAS*, **338**, 609
- Murray, C. E., et al. 2015, *ApJ*, **808**, 41
- Murray, C. E., et al. 2018, *ApJS*, **238**, 14
- Nguyen, H., et al. 2019, *ApJ*, **880**, 141
- Nidever, D. L., Majewski, S. R., & Butler Burton, W. 2008, *ApJ*, **679**, 432
- Nidever, D. L., Majewski, S. R., Butler Burton, W., & Nigra, L. 2010, *ApJ*, **723**, 1618
- Panessa, M., et al. 2023, *MNRAS*, **523**, 6138
- Park, G., et al. 2023, in *IAU Symposium*, Vol. 373, *Resolving the Rise and Fall of Star Formation in Galaxies*, ed. T. Wong, & W.-T. Kim, 81
- Peek, J. E. G., et al. 2011, *ApJS*, **194**, 20
- Peek, J. E. G., et al. 2018, *VizieR Online Data Catalog*, *J/ApJS/234/2*
- Price-Whelan, A. M., et al. 2019, *ApJ*, **887**, 19
- Putman, M. E., Staveley-Smith, L., Freeman, K. C., Gibson, B. K., & Barnes, D. G. 2003, *ApJ*, **586**, 170
- Richter, P., et al. 2013, *ApJ*, **772**, 111
- Richter, P., et al. 2018, *ApJ*, **865**, 145
- Richter, P., Sembach, K. R., Wakker, B. P., & Savage, B. D. 2001, *ApJL*, **562**, L181
- Rolleston, W. R. J., Trundle, C., & Dufton, P. L. 2002, *A&A*, **396**, 53
- Roman-Duval, J., et al. 2014, *ApJ*, **797**, 86
- Rybarczyk, D. R., et al. 2022a, *ApJ*, **926**, 190
- Rybarczyk, D. R., et al. 2022b, *ApJ*, **928**, 79
- Sembach, K. R., Howk, J. C., Savage, B. D., & Shull, J. M. 2001, *AJ*, **121**, 992
- Stanimirović, S., et al. 2008, *ApJ*, **680**, 276
- Stanimirovic, S., Gallagher, J. S., I., & Nigra, L. 2010, *SerAJ*, **180**, 1
- Stanimirović, S., Murray, C. E., Lee, M.-Y., Heiles, C., & Miller, J. 2014, *ApJ*, **793**, 132
- Sternberg, A., McKee, C. F., & Wolfire, M. G. 2002, *ApJS*, **143**, 419
- Wakker, B. P. 2001, *ApJS*, **136**, 463
- Wakker, B. P. 2006, *ApJS*, **163**, 282
- Wang et al. 2019, *MNRAS*, **486**, 4
- Weiner, B. J. & Williams, T. B. 1996, *AJ* **111**, 1156
- Westmeier, T. 2018, *MNRAS*, **474**, 289
- Wolfire, M. G., McKee, C. F., Hollenbach, D., & Tielens, A. G. G. M. 1995, *ApJ*, **453**, 673
- Zaritsky, D., et al. 2020, *ApJL*, **905**, L3